



HAL
open science

Interactions of REF1 and SRPP1 rubber particle proteins from *Hevea brasiliensis* with synthetic phospholipids: Effect of charge and size of lipid headgroup

Kanthida Wadeesirisak, Sabine Castano, Laurent Vaysse, Frédéric Bonfils, Frédéric Peruch, Kittipong Rattanaporn, Siriluck Liengprayoon, Sophie Lecomte, Céline Bottier

► **To cite this version:**

Kanthida Wadeesirisak, Sabine Castano, Laurent Vaysse, Frédéric Bonfils, Frédéric Peruch, et al.. Interactions of REF1 and SRPP1 rubber particle proteins from *Hevea brasiliensis* with synthetic phospholipids: Effect of charge and size of lipid headgroup. *Biochemical and Biophysical Research Communications*, 2023, 679, pp.205-214. 10.1016/j.bbrc.2023.08.062 . hal-04273044

HAL Id: hal-04273044

<https://hal.science/hal-04273044>

Submitted on 7 Nov 2023

HAL is a multi-disciplinary open access archive for the deposit and dissemination of scientific research documents, whether they are published or not. The documents may come from teaching and research institutions in France or abroad, or from public or private research centers.

L'archive ouverte pluridisciplinaire **HAL**, est destinée au dépôt et à la diffusion de documents scientifiques de niveau recherche, publiés ou non, émanant des établissements d'enseignement et de recherche français ou étrangers, des laboratoires publics ou privés.

1 **Interactions of REF1 and SRPP1 rubber particle proteins from *Hevea brasiliensis* with**
2 **synthetic phospholipids: effect of charge and size of lipid headgroup**

3
4 Kanthida Wadeesirisak^a, Sabine Castano^b, Laurent Vaysse^{c,d}, Frédéric Bonfils^{c,d}, Frédéric Peruch^e,
5 Kittipong Rattanaporn^f, Siriluck Liengprayoon^g, Sophie Lecomte^{b*} and Céline Bottier^{c,d*}

6
7 ^a Institute of Food Research and Product Development, Kasetsart University, 10900 Bangkok,
8 Thailand

9 ^b Univ. Bordeaux, CNRS, Bordeaux INP, CBMN, UMR5248, F-33600, Pessac, France

10 ^c CIRAD, UPR BioWooEB, F-34398 Montpellier, France

11 ^d BioWooEB, Univ Montpellier, CIRAD, Montpellier, France

12 ^e Univ. Bordeaux, CNRS, Bordeaux INP, LCPO, UMR 5629, F-33600, Pessac, France

13 ^f Department of Biotechnology, Faculty of Agro-Industry, Kasetsart University, 10900 Bangkok,
14 Thailand

15 ^g Kasetsart Agricultural and Agro-Industrial Product Improvement Institute, Kasetsart University,
16 10900 Bangkok, Thailand

17
18 ***CORRESPONDING AUTHORS:**

19
20 **Dr. Sophie Lecomte**

21 sophie.lecomte@u-bordeaux.fr

22 Institut de Chimie et Biologie des Membranes et Nano-objets

23 CNRS, CBMN, UMR 5248

24 Allée Geoffroy Saint-Hilaire

25 33600 Pessac

26 France

27 Tel: + 33 (0)5 40 00 68 20

28
29 **Dr. Céline Bottier**

30 celine.bottier@cirad.fr

31 CIRAD/UR BioWooEB

32 TA B-62 / 16

33 Maison de la Technologie / Bât 16

34 73 rue Jean-François Breton

35 34398 Montpellier Cedex 05

36 France

37 Tel: +33 (0)4 67 61 49 91

38
39 **KEYWORDS**

40 *Hevea brasiliensis*, rubber particle proteins, rubber elongation factor, small rubber particle
41 protein, anionic phospholipids, latex coagulation

42
43
44 **ABSTRACT**

45 According to the fatty acid and headgroup compositions of the phospholipids (PL) from
46 *Hevea brasiliensis* latex, three synthetic PL were selected (*i.e.* POPA: 1-palmitoyl-2-oleoyl-
47 sn-glycero-3-phosphate POPC: 1-palmitoyl-2-oleoyl-sn-glycero-3-phosphocholine and
48 POPG: 1-palmitoyl-2-oleoyl-sn-glycero-3-phosphoglycerol) to investigate the effect of PL

49 headgroup on the interactions with two major proteins of *Hevea* latex, *i.e.* Rubber Elongation
50 Factor (REF1) and Small Rubber Particle Protein (SRPP1). Protein/lipid interactions were
51 screened using two models (lipid vesicles in solution or lipid monolayers at air/liquid
52 interface). Calcein leakage, surface pressure, ellipsometry, microscopy and spectroscopy
53 revealed that both REF1 and SRPP1 displayed stronger interactions with anionic POPA and
54 POPG, as compared to zwitterionic POPC. A particular behavior of REF1 was observed
55 when interacting with POPA monolayers (*i.e.* aggregation + modification of secondary
56 structure from α -helices to β -sheets, characteristic of its amyloid aggregated form), which
57 might be involved in the irreversible coagulation mechanism of *Hevea* rubber particles.

58
59

INTRODUCTION

60 *Hevea brasiliensis* (Willd. Ex A. Juss) Müll. Arg (*para* rubber tree), a tropical plant
61 belonging to the *Euphorbiaceae* family, is the only commercial source of natural rubber
62 (NR). NR exhibits very specific properties that are not mimicked by synthetic rubbers such as
63 low heat build-up and crystallization under strain. However, it also suffers from drawbacks,
64 such as the variability of its properties. NR originates from the latex of *H. brasiliensis* tree,
65 which is a colloidal suspension of rubber particles (RP) and lutoids in cytoplasmic serum.
66 The micrometric and spherical RP are made of a polyisoprene core surrounded by a
67 lipid/protein biomembrane [1-4]. Interestingly, the RP from *H. brasiliensis* latex have a
68 bimodal size distribution, with large rubber particles (LRP, diameter ~ 0.4 – 1.0 μm) and small
69 rubber particles (SRP, diameter ~ 0.1 – 0.4 μm) [5-7]. When latex is processed into NR, it is
70 not clear whether the RP retain their structure and/or composition in dry NR. Wu *et al.* used a
71 super-resolution fluorescence imaging technique to characterize latex and NR samples, and
72 they suggested that there is some sort of interaction between proteins and lipids in dry NR
73 [8]. Therefore, a precise description of the RP membrane at latex stage is needed to better
74 understand the interactions between polyisoprene chains, lipids and proteins in dry NR. This
75 would help to better control the variability of NR quality and understand its structuration
76 dynamics.

77 Among the many proteins associated with *H. brasiliensis* RP [9], two abundant proteins
78 are important for their role in rubber biosynthesis: Rubber Elongation Factor (REF) and
79 Small Rubber Particle Protein (SRPP) [10-13]. These two hydrophobic proteins are found on
80 the surface of RP [14]. Ten isoforms of SRPP (SRPP1–10) and eight isoforms of REF
81 (REF1–8) have been identified in the almost complete *H. brasiliensis* genome (93.8%, 1.37
82 Gb), but the expression of REF1 and SRPP1 genes prevails in latex [15]. Previously, we have
83 carried out several studies to describe the organization/structure of REF1 and SRPP1 proteins
84 at the surface of RP by studying lipid/protein interactions in Langmuir films. In this original
85 approach, the lipid/protein membrane surrounding the poly(*cis*-1,4-isoprene) core of the
86 rubber particle was mimicked by a lipid Langmuir monolayer formed at the air/water
87 interface [16] and interacting with REF1 and SRPP1 proteins. We first applied this strategy to
88 study the interactions of recombinant REF1 and SRPP1 proteins with synthetic lipids [17,

89 18]. We later investigated the interactions of both proteins with native lipids extracted from
90 latex and separated into three types: neutral lipids (NL), glycolipids (GL) and phospholipids
91 (PL) [19]. It was shown that both REF1 and SRPP1 proteins have different behaviors
92 depending on the type of lipid they bind to. In particular, while the secondary structure of
93 REF1 in α -helices is maintained when interacting with native PL and GL, it switches to β -
94 sheets in the presence of native NL.

95 Plant lipids are complex mixtures of different lipid species [20]. This complexity is also
96 observed in the latex of *H. brasiliensis*, where the presence of NL, GL and PL was reported
97 [21-23]. PL of *H. brasiliensis* latex were shown to contain different species with various
98 headgroups and esterified acyl chains [22]. As structural lipids of the RP membrane [2, 24],
99 PL interact with rubber proteins REF1 and SRPP1 at the RP membrane. Various headgroup
100 types and fatty acyl chain lengths were identified within PL family [22]. This diversity in
101 headgroup and fatty acyl chain was shown to impact the PL-binding ability of TbSRPP1-3,
102 three isoforms of SRPP from *T. brevicorniculatum*, another rubber-producing plant [25]. The
103 screening of the affinity of TbSRPPs for different PL revealed a preference for negatively
104 charged headgroups and C18:2/C16:0 fatty acid chains.

105 In this study, we investigated the interaction between synthetic PL and recombinant REF1
106 or SRPP1 proteins. We determined the headgroup and fatty acid compositions of native PL
107 from *Hevea* latex and we selected three synthetic PL (*i.e.* POPC, POPA, POPG). These three
108 synthetic PL have exactly the same acyl chains (PO: 1-palmitoyl-2-oleoyl, C16:0/C18:1) but
109 various headgroups (phosphocholine, phosphate and phosphoglycerol). Phosphocholine (PC)
110 (zwitterionic) and phosphate (PA) (anionic) were chosen because of their important amount
111 in *Hevea* latex. Anionic phosphoglycerol (PG) was also chosen, even though it is not found in
112 latex, to investigate the effects of size (small POPA *vs* large POPG) and charge (zwitterionic
113 POPC *vs* anionic POPG) of the headgroup. We performed an affinity screening to
114 characterize the interactions of RP proteins with the selected synthetic PL. We used
115 ellipsometry, BAM, PM-IRRAS and fluorescence (calcein leakage) to measure these
116 interactions. The lipid headgroup was shown to have a strong impact on the behavior of both
117 REF1 and SRPP1. REF1 and SRPP1 induced strong calcein leakage in POPA and POPG
118 LUV. The strong interaction with POPA led to an aggregation of REF1 and formation of β -
119 sheets, similar to its amyloid-like structure. This mechanism may be important when REF1
120 interacts with lutoids, some intracellular organelles found in latex, as their membranes are
121 enriched in phosphatidic acid [26]. It has been proposed that the interactions of REF1 with
122 phosphatidic acid-enriched lutoid membranes might result in a switch of REF1 structure to its
123 amyloid-aggregated form, which would be involved in the irreversible coagulation
124 mechanism of *Hevea brasiliensis* RP.

125 126 **EXPERIMENTAL SECTION**

127 **1. Native phospholipids from *Hevea* latex**

128 *Hevea brasiliensis* rubber trees of certified RRIM600 clone planted in 2002 and tapped for
129 the first time in 2009 (tapping system S/2, 2d/3) were selected from a plantation belonging to
130 Visahakit Thai Rubber Co., Ltd., Chanthaburi, Thailand. The latex sampling details, the
131 extraction and purification methods of PL and the determination of the lipid composition of
132

133 latex (total lipids, phospholipids, glycolipids, neutral lipids) have been described previously
134 [19].

135

136 **2. Commercial phospholipids**

137 Synthetic PL used for Langmuir film studies were from Avanti (USA): 1-palmitoyl-2-
138 oleoyl-sn-glycero-3-phosphate (sodium salt) (POPA), 1-palmitoyl-2-oleoyl-sn-glycero-3-
139 phosphocholine (POPC), and 1-palmitoyl-2-oleoyl-sn-glycero-3-phospho-(1'-rac-glycerol)
140 (sodium salt) (POPG).

141 In addition, five PL were used as standards to determine the headgroup composition of
142 native phospholipids of *Hevea* latex: 1-palmitoyl-2-oleoyl-sn-glycero-3-phosphatidic acid
143 (Larodan, Malmö, Sweden), L- α -phosphatidylinositol sodium salt from soybean (PI) (Sigma-
144 Aldrich, USA), phosphatidylcholine from egg yolk (PC) (Sigma-Aldrich, USA), L- α -
145 lysophosphatidylcholine from egg yolk (LPC) (Sigma-Aldrich, USA) and L- α -
146 phosphatidylethanolamine from egg yolk (PE) (Sigma, USA).

147

148 **3. Fatty acid composition of native phospholipids of latex by GC-FID**

149 To obtain fatty acids from PL, around 20 mg of PL was saponified by mixing with 5 mL
150 of a mixture of methanol/6M NaOH (9:1, v/v) and refluxed at 80 °C for 1.5 hours. After
151 cooling, 10 mL of water was added and the unsaponifiable fraction was separated with 3 x 10
152 mL of n-hexane. The fatty acid containing aqueous bottom phase was acidified with 0.6 mL
153 of 6 M HCl (pH below 3) and the free fatty acids were extracted with 3 x 10 mL of n-hexane.
154 After evaporation, the obtained total fatty acids were methylated by adding 5 mL of 2% of
155 concentrated H₂SO₄ in methanol and refluxed at 80 °C for 1.5 hours and 0.5 mL of water was
156 added once the solution was cooled down. The derived fatty acid methyl esters (FAME) were
157 extracted with 3 x 5 mL of n-hexane and evaporated. The concentration of FAME was
158 adjusted to 1 mg.mL⁻¹ and injected to GC-FID. A Shimadzu GC17A gas chromatograph
159 (Shimadzu Co., Kyoto, Japan) equipped with a fused silica capillary column BPX70 (30 m,
160 i.d. 0.25 mm, film thickness 0.25 μ m, SGE, Victoria, Australia) and a Shimadzu AOC20i
161 automatic injector (injected volume 1 μ L) were used. The initial linear velocity of helium in
162 the column was 34 cm.sec⁻¹. The temperature of the split injector (split ratio 1:15) and of the
163 flame ionization detector was 250 °C and 280 °C, respectively. Oven temperature was
164 programed to start at 160 °C for 0.5 min, and then increased to 200 °C at 10 °C.min⁻¹ and
165 kept constant for 4 min. Data acquisition was performed using the GC solution v 2.10
166 software (Shimadzu Co., Kyoto, Japan). Calibration curve was performed using fatty acid
167 methyl ester (FAME) standard mixtures containing C14-C20 fatty acids at total
168 concentrations ranging from 0.5 to 10 mg.mL⁻¹.

169

170 **4. Headgroup composition of native phospholipids of latex by HPLC-MS**

171 The separation and identification of phospholipid species was carried out with normal-
172 phase liquid chromatography using a Waters Alliance 2695 separation module (Waters Corp.,
173 Massachusetts, United States). This module was equipped with an Atlantis HILIC Silica
174 column (150 mm x 2.1 mm, 3 μ m particles size, Waters, Ireland) thermostated at 30 °C and
175 coupled to a Waters SQ Detector 2 mass spectrometer with a combined ESI/APCI/ESCI

176 probe. Both lipid standards and samples were solubilized in chloroform/methanol (2:1). A
177 volume of 5 μL of sample ($1 \text{ mg}\cdot\text{mL}^{-1}$) or lipid standard solutions in a range from 0 to 1.0
178 $\text{mg}\cdot\text{mL}^{-1}$ (concentrations: 0.01, 0.05, 0.1, 0.2, 0.4, 0.6, 0.8, and $1.0 \text{ mg}\cdot\text{mL}^{-1}$) were injected
179 using the Water Alliance 2695 autosampler.

180 The separation was performed with a ternary mixture mobile phase consisting of (A)
181 methanol with 0.1% ammonium hydroxide (v/v), (B) chloroform with 0.1% ammonium
182 hydroxide (v/v), and (C) deionized water with 0.1% ammonium hydroxide (v/v) with the
183 flow rate of $0.25 \text{ mL}\cdot\text{min}^{-1}$. Separation was obtained by using gradient starting at 24.5% of A,
184 75% of B and 0.5% of C. Then the ratios are linearly changed to 50% of A, 44.5% of B and
185 5.5% of C within 10 min and held isocratically for 20 min. The total chromatographic run
186 time was 40 min. The mass spectrometer was operated under positive electrospray ionization
187 (ESI+) (capillary voltage 5 kV; cone voltage 70 V; source temperature $150 \text{ }^\circ\text{C}$; desolvation
188 temperature $250 \text{ }^\circ\text{C}$; desolvation nitrogen flow $260 \text{ L}\cdot\text{h}^{-1}$; cone nitrogen flow $30 \text{ L}\cdot\text{h}^{-1}$) and
189 negative electrospray ionization (ESI-) (40 and 90 V of cone voltage with the same other
190 parameters). The full scan mass spectrum was acquired in the mass range between m/z 190
191 and 1200.

192

193 **5. Expression and purification of REF1 and SRPP1 proteins**

194 Recombinant *Hevea brasiliensis* REF1 and SRPP1 proteins were produced in *Escherichia*
195 *coli* and purified as described previously by Berthelot *et al.* [17]. Briefly, recombinant *Hevea*
196 *brasiliensis* REF1 and SRPP1 proteins were produced in *Escherichia coli* BL21 (DE3) pLysS
197 Gold cells. Bacteria were grown to 0.7 OD in $2\times$ YT medium (16 g/L tryptone, 10 g/L yeast
198 extract, and 5.0 g/L NaCl), and expression was induced by addition of 1 mM isopropyl-D-
199 thiogalactoside (Euromedex, Souffelweyersheim, France). After 4 h induction, cells were
200 harvested by centrifugation and frozen at $-20 \text{ }^\circ\text{C}$. Overexpression of SRPP1 and REF1
201 caused inclusion body formation. Cells were sonicated $5 \times 1 \text{ min}$ in buffer A (150 mM NaCl
202 and 100 mM Tris-HCl, pH 8.0). The lysate was centrifuged for 30 min at $20,000g$. The pellet
203 was washed in the buffer A and re-suspended in denaturing buffer (8 M urea in buffer A).
204 The lysate was incubated with 3 mL Ni-NTA resin (InVitrogen, ThermoScientifique, Illkirch,
205 France) for 2 h at room temperature. The resin was then washed twice with 35 mL of 8 M
206 urea/buffer A, by centrifuging 10 min at $900g$. The proteins were eluted from the resin in the
207 same buffer containing 250 mM imidazole (Euromedex). Protein samples were pooled and
208 dialyzed against 25 mM Tris/HCl pH 8.0 and kept aliquoted at $-80 \text{ }^\circ\text{C}$.

209

210 **6. Characterization of the interactions between lipids and protein**

211 *6.1 Calcein leakage measurements of large unilamellar vesicles (LUV)*

212 The ability of proteins to interact with large unilamellar vesicles (LUV) results in a
213 destabilization of their membrane and thus in a calcein release in the medium which is
214 recorded by fluorescence. Calcein leakage experiments were performed by monitoring the
215 fluorescence signal after adding REF1 and SRPP1 proteins to LUV made from pure POPC
216 and POPG lipids. However, due to the geometry of POPA lipid (small headgroup with large
217 fatty acid chains) [27], it was not possible to prepare LUV made of POPA only. Thus, for
218 POPA, LUV were prepared from an equimolar mixture of POPA and POPC. To form LUV,
219 dried lipid films were hydrated with buffer containing calcein (70 mM in TBS 1X pH 7.4,

220 TBS: Tris 20 mM, NaCl 150 mM) and dispersion was run through five freeze/thawing cycles
221 and passed through a mini-extruder equipped with two stacked 0.1 μm polycarbonate filters
222 (Avanti, USA). The sizes of LUV were determined to be around 120 nm by dynamic light
223 scattering (DynaPro Nanostar, US). The lipid concentration was calculated by phosphate
224 dosage [28].

225 Fluorescence measurements were made with a microplate reader (TECAN infinite
226 M1000PRO). After the addition of the reactants, the 384-well microplate (Grenier Flat
227 bottom, black polystyrene) was shaken just before measurement. Data were collected every 1
228 h at 25 $^{\circ}\text{C}$, λ excitation at 485 nm and λ emission at 515 nm. Lipid concentration was set at
229 100 μM and concentration of proteins varied from 0.01 μM to 50 μM (total volume 30 μL).
230 After 24 hours, 1 μL of 10% Triton X-100 (Sigma) solution was added to achieve complete
231 liposome leakage. The percentage of calcein release was calculated according to the
232 following equation: $L(t) = [(F_t - F_0) / (F_{\text{max}} - F_0)] \times 100$, where $L(t)$ is the percentage of the
233 calcein released (%), F_t is the measured fluorescence intensity at time t , F_0 is the fluorescence
234 intensity at time $t = 0$ and F_{max} is the fluorescence intensity after addition of Triton X-100.
235 Each experiment was repeated two times.

236

237 6.2 Surface tension

238 Adsorption of proteins below air/buffer or lipid/buffer interface was followed by surface
239 pressure (Π) measurement. Experiments were performed at 25 ± 1 $^{\circ}\text{C}$ on a circular Teflon
240 trough of 20.4 cm^2 filled with 8 mL of subphase (TBS 1X buffer pH 7.4). The surface
241 pressure (Π) was measured with a plate of Whatman filter paper held by a Nima Wilhelmy
242 balance. The interaction of proteins with lipid films was performed in two steps. First, the
243 lipids were spread at the air-buffer interface from chloroform/methanol (4:1 v/v) solution at 1
244 $\text{mg}\cdot\text{mL}^{-1}$ to reach the desired surface pressure (28 $\text{mN}\cdot\text{m}^{-1}$). Second, proteins were injected at
245 a final concentration of 2 μM into the subphase using a microsyringe. The surface pressure
246 was measured continuously during protein adsorption in the lipid monolayer until an
247 equilibrium pressure was reached (plateau). The difference between the initial surface
248 pressure of the lipid (Π_i) and the surface pressure reached at the plateau (Π_p) gives the
249 surface pressure increase ($\Delta\Pi = \Pi_p - \Pi_i$). Each experiment was repeated at least 2 times and
250 reported values are the means with their corresponding standard deviations.

251

252 6.3 Ellipsometry and Brewster angle microscopy (BAM)

253 The thickness of the films formed at the air-buffer interface was determined on a 6 mL
254 Teflon trough using a NFT IELI2000 ellipsometer (Göttingen, Germany) equipped with a
255 doubled frequency Nd-Yag laser (532 nm, 50 mW), a polarizer, an analyzer, and a CCD
256 camera. The imaging ellipsometer works at an incidence angle close to the Brewster angle
257 (54.58°) and it operates on the principle of classical null ellipsometry. The morphology of
258 films at the air-buffer interface was observed by the CCD camera. The spatial resolution was
259 about 1 μm and the size of BAM images was 450×600 μm^2 with the $\times 10$ magnification
260 objective used. The angles of the polarizer, compensator, and analyzer that obtained the null
261 condition allow one to get the (Δ , Ψ) ellipsometric angles which are related to the optical
262 properties of the sample [29, 30]. For ultrathin films, Δ is proportional to the film thickness.

263 The value of the film thickness mainly depends on the refractive index used. Since it is
 264 difficult to determine an accurate experimental refractive index value, we used the same
 265 average value of the refractive index 1.45 for both lipid layers and proteins to perform
 266 thickness estimations. The BAM images presented in the various figures were corrected from
 267 the tilt angle observation. Note that a shutter was used with various timing to avoid camera
 268 saturation.

269

270 6.4 Polarization modulated-infrared reflection adsorption spectroscopy (PM-IRRAS)

271 Polarization modulated-infrared reflection-adsorption spectra were recorded on a Nicolet
 272 (Madison, WI) Nexus 870 spectrometer equipped with a HgCdTe (MCT) detector (SAT,
 273 France) and cooled at 77 K by liquid nitrogen at a resolution of 8 cm⁻¹ by adding 600 scans.
 274 Details of PM-IRRAS experiments were previously described [18, 31]. PM-IRRAS spectra
 275 were normalized by the TBS 1X buffer pH 7.4 spectrum or lipid spectrum. The room
 276 temperature was regulated at 25 ± 1 °C. Each experiment was repeated at least 2 times.

277

278 RESULTS AND DISCUSSION

279

280 1. Linoleyl (C18:2) and phosphocholine are the major acyl chain and the major 281 headgroup of the phospholipid extract of *Hevea latex*, respectively

282 The knowledge of the detailed native PL composition of *Hevea latex* was necessary to
 283 select synthetic PL. The latex from RRIM600 clone contained 2.71% (w/w dry rubber) of
 284 extractable lipids [19], which were composed of: 45 ± 3 % of neutral lipids (NL), 32 ± 1% of
 285 phospholipids (PL) and 23 ± 2% glycolipids (GL).

286 The fatty acid (FA) composition of saponified latex PL extract is reported in Table 1.
 287 Linoleic acid was found to be the major FA (49.7%). The other FA were found in the
 288 following order of decreasing abundance: oleic (22.4%), stearic (13.6%), palmitic (9.2%),
 289 linolenic (2.9%), palmitoleic (1.1%), arachidic (1.1%) and furanoic (0.2%). Although those
 290 data agree with a previous study [22], one important difference was noticed regarding the
 291 proportion of oleic acid which was found to have doubled as compared to the previous study.
 292 This is believed to be mostly due to a modification of the extraction procedure applied in the
 293 present study, specifically the use of SPE technique [19], which likely preserved the lipid
 294 extract from transesterification toward methyl esters that could preferentially target the C18:2
 295 species. Additionally, the trees used in the two studies were of different ages, which could
 296 also have impacted the lipid composition [32].

297

Fatty acids	FA composition of PL extract from latex (% w/w of total PL FA)
Myristic acid C14:0	-
Palmitic acid C16:0	9.2 ± 0.02
Palmitoleic acid C16:1	1.0 ± 0.02
Stearic acid C18:0	13.6 ± 0.02
Oleic acid C18:1	22.4 ± 0.02
Linoleic acid C18:2	49.7 ± 0.02
Linolenic acid C18:3	2.9 ± 0.02

Arachidic acid C20:0	1.0 ± 0.02
Furanoic acid	0.2 ± 0.03

298 **Table 1.** Fatty acid (FA) composition of saponified phospholipids (PL) extracted from fresh latex of
 299 RRIM600 clone. The standard error was obtained from 3 saponifications of one PL sample.

300

301 FA composition of latex PL was used to select the FA chains of synthetic PL. Linoleic and
 302 oleic acids were found to be the most abundant FA species in latex PL (Table 1). However,
 303 synthetic PL with the combination of these two FA are not commercially available, while in
 304 contrast, PL species that associate a palmitoyl chain to an oleyl one are the most often used in
 305 Langmuir model membrane studies [33, 34]. Indeed, these lipids have different chain lengths,
 306 with a saturated chain associated to a non-saturated one, making them good models to mimic
 307 the variety of native lipid mixtures [35]. Therefore, we chose to associate a palmitoyl chain to
 308 an oleyl one, which is a good compromise for this study, as these two FA roughly represent
 309 one third of the total FA found in latex PL extract (Table 1).

310 The headgroup composition of the latex PL extract is reported in Table 2. The main
 311 species detected among PL headgroups of RRIM600 latex were phosphocholine (50%),
 312 followed by phosphoethanolamine (19%), phosphate (16%) and phosphoinositol (15%).

313

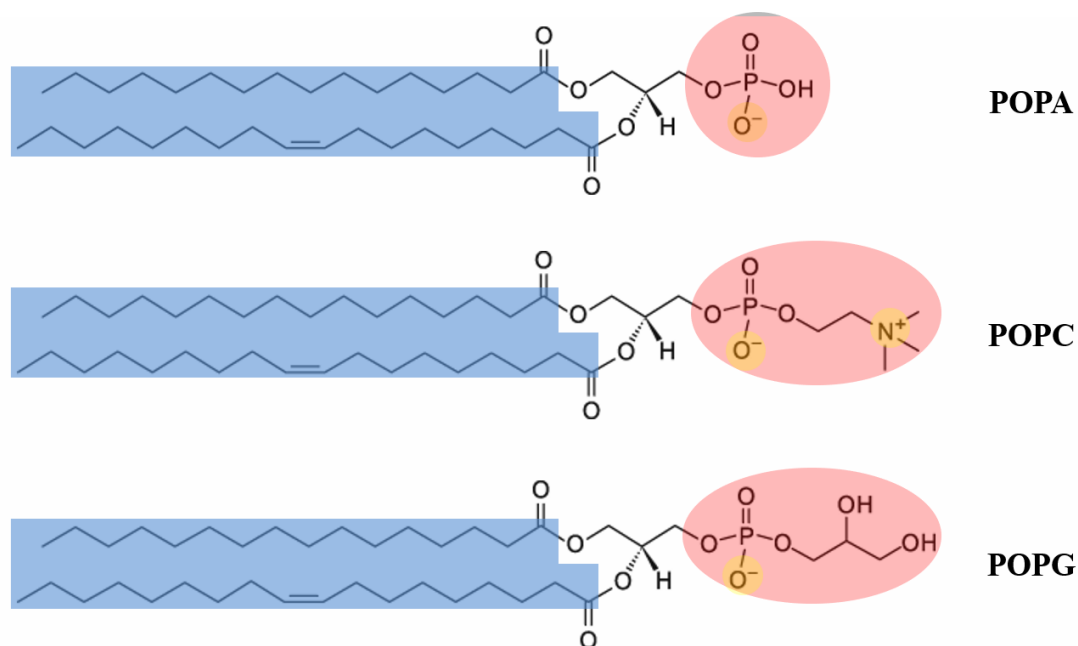
PL headgroup	Headgroup composition of PL extract from RRIM600 latex (% w/w of total PL headgroups)
Phosphocholine	50 ± 2
Phosphoethanolamine	19 ± 3
Phosphate	16 ± 2
Phosphoinositol	15 ± 1

314 **Table 2.** Headgroup composition of phospholipids (PL) extracted from fresh latex of RRIM600 clone.
 315 The standard error was obtained from 3 injections of one PL sample.

316

317 The headgroup composition of latex PL extract, given in Table 2, was used to select the
 318 headgroups of synthetic PL. Both phosphocholine and phosphate headgroups were found in
 319 significant amounts in native PL from latex. Interestingly, both phosphocholine and
 320 phosphate have opposite properties that are valuable for our research purpose:
 321 phosphocholine is a large zwitterionic headgroup, while phosphate is a small negatively-
 322 charged headgroup (charge -1 at pH 7.4, [36]). Moreover, although the lipid headgroup
 323 phosphoglycerol was not detected in native PL of latex, it was included in this study because
 324 its size is comparable to that of phosphocholine headgroup, while it is negatively charged as
 325 phosphate (charge -1, at pH 7.4, [36]). Figure 1 shows the chemical structures of the three
 326 selected synthetic PL: POPA (1-palmitoyl-2-oleoyl-sn-glycero-3-phosphate), POPC (1-
 327 palmitoyl-2-oleoyl-sn-glycero-3-phosphocholine) and POPG (1-palmitoyl-2-oleoyl-sn-
 328 glycero-3-phosphoglycerol). REF1 and SRPP1 proteins were studied for their interactions
 329 with those three synthetic PL in the form of vesicles and monolayers.

330



331
 332 **Figure 1.** Chemical structures of the three synthetic PL chosen to be studied in interaction with REF1
 333 and SRPP1 proteins: POPA (1-palmitoyl-2-oleoyl-sn-glycero-3-phosphate), POPC (1-palmitoyl-2-
 334 oleoyl-sn-glycero-3-phosphocholine) and POPG (1-palmitoyl-2-oleoyl-sn-glycero-3-
 335 phosphoglycerol). A color code was added: blue rectangles correspond to acyl chains (similar for the
 336 3 lipids: C16:0/C18:1), red areas show lipid headgroups and yellow patches highlight charges at pH
 337 7.4 (POPA and POPG are negatively charged while POPC is zwitterionic).

338

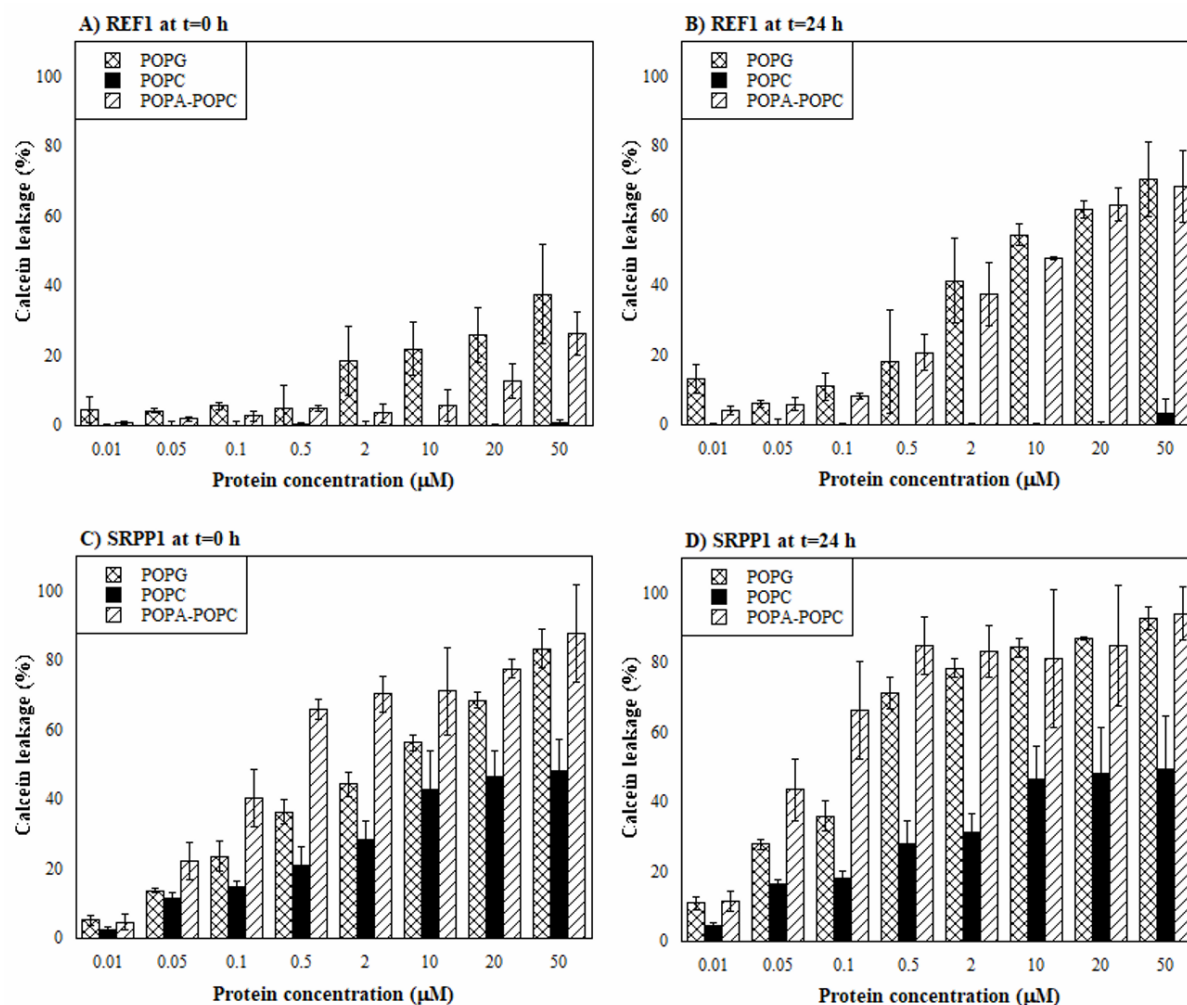
339

2. SRPP1 interacts more strongly than REF1 with LUV of anionic PL

340 The effect of the RP proteins REF1 and SRPP1 on PL LUV were studied by fluorescent
 341 calcein leakage measured at $t=0$ h and $t=24$ h. Calcein was encapsulated in POPC or POPG
 342 LUV. However, due to the geometry of POPA lipid (small headgroup with large fatty acid
 343 chains) [27], it was not possible to prepare LUV made of pure POPA. Therefore, to study the
 344 protein interactions with POPA, we used LUV prepared from an equimolar mixture of POPA
 345 and POPC. The percentage of released calcein from POPC, POPG and POPA/POPC LUV at
 346 $t=0$ h and $t=24$ h induced by REF1 or SRPP1 is shown in Figure 2.

347 Interestingly, for all three lipids (POPG, POPC, POPA/POPC), all protein concentrations
 348 (0.01 to 50 μM) and both times ($t=0$ h and $t=24$ h), SRPP1 systematically induced a higher
 349 calcein leakage from LUV than REF1, although the values between REF1 and SRPP1 were
 350 not always statistically different. Moreover, the comparison of the curves at $t=0$ h and $t=24$ h
 351 shows that REF1 acts in a time-dependent manner (Figures 2A vs 2B), while SRPP1 affects
 352 the integrity of the LUV more instantaneously (Figures 2C vs 2D). The stronger disruption of
 353 LUV (120 nm) by SRPP1 than REF1 might reflect the preference of SRPP1 for binding to
 354 smaller RP. This is in agreement with the fact that SRPP1 and REF1 mostly bind to SRP (<
 355 0.2 μm) and LRP (> 0.3 μm), respectively [41].

356



357
 358 **Figure 2.** Fluorescent calcein leakages (with standard deviations) measured at t=0 h (A, C) and t=24
 359 h (B, D) from LUV (100 μM in TBS 1X pH 7.4) made of POPC, POPA/POPC (1:1) and POPG in the
 360 presence of the proteins REF1 (A, B) and SRPP1 (C, D) injected at various concentrations (0.01 to 50
 361 μM).

362
 363 REF1 did not induce any calcein leakage from POPC LUV neither at t=0 h (Figure 2A) or
 364 t=24 h (Figure 2B). When POPA was added to POPC (in an equimolar mixture 1:1) to form
 365 LUV, calcein leakages ranging from 1.0 to 26.5% and 4.3 to 68.3% were measured at t=0 h
 366 and t=24 h, respectively, for REF1 concentrations from 0.01 to 50 μM . Therefore, this
 367 suggests the absence of interaction between REF1 and POPC LUV, rather than an
 368 aggregation of REF1 outside the LUV. In contrast to REF1, SRPP1 induced leakage of POPC
 369 LUV (Figures 2C and 2D), as indicated by leakages increasing from 2.3 to 48.3% at t=0 h,
 370 and from 4.6 to 49.3% at t=24 h, when SRPP1 concentration was increased from 0.01 to 50
 371 μM . The calcein leakages of POPC LUV measured with SRPP1 were significantly higher
 372 than the ones measured with REF1 at both times and for all protein concentrations.

373 Higher calcein leakages were previously measured from EggPC LUV in the presence of
 374 REF1 and SRPP1, *i.e.* 35% and 70%, respectively [18]. The two major acyl chains in EggPC
 375 are C16:0 (33%) and C18:1 (32%), which are the same as those in POPC. EggPC also
 376 contains 20% of C18:2, which suggests that both REF1 and SRPP1 proteins have a
 377 preference for this acyl species. As a polyunsaturated acyl chain, C18:2 can influence

378 membrane fluidity and stereochemistry, thereby facilitating hydrophobic interactions between
379 the hydrophobic proteins REF1 and SRPP1 and the acyl chains of the LUV membrane. This
380 mechanism could explain the enhanced LUV disruption observed for EggPC [18], as
381 compared to what is observed in the present study for POPC. Protein affinity for specific acyl
382 chains has been shown for other proteins. For example, three *T. brevicorniculatum* SRPP
383 proteins (SRPP3–5), have preferred interactions with C16:0/C18:2 acyl chains, and the
384 authors proposed that they may bind to RP via pockets of unsaturated PC [25].

385 Compared to zwitterionic POPC LUV, REF1 interacts more strongly with both anionic
386 POPA/POPC and POPG LUV, at both times $t=0$ h (Figure 2A) and $t=24$ h (Figure 2B). With
387 both anionic LUV types, REF1 acts in a dose-dependent manner. Indeed, at $t=0$ h, and for
388 REF1 concentrations varying from 0.01 to 50 μM , the calcein leakages from POPG LUV
389 ranged from 4.6 to 37.6% (Figure 2A), and those from POPA/POPC LUV ranged from 1.0 to
390 26.5% (Figure 2A). At $t=24$ h, REF1 concentrations from 0.01 to 50 μM induced calcein
391 leakages of 13.3 to 70.4% for POPG (Figure 2B) and 4.3 to 68.3% for POPA/POPC (Figure
392 2B). At both times ($t=0$ h, $t=24$ h) and for all protein concentrations (0.01 to 50 μM), the
393 calcein leakages induced by REF1 were in the same order for POPG as for POPA/POPC
394 LUV. For SRPP1, as observed for REF1, the incorporation of POPA into POPC (1:1)
395 (Figures 2C and 2D) significantly enhanced the calcein leakage from LUV by the protein, at
396 both times $t=0$ h and $t=24$ h. The calcein leakage values from POPG LUV by SRPP1 were in
397 the same range as those from POPA/POPC LUV. When increasing SRPP1 concentration
398 from 0.01 to 50 μM , the calcein leakages increased from 5.3 to 83.4% for POPG and 4.7 to
399 87.7% for POPA/POPC at $t=0$ h, and from 11.0 to 92.7% for POPG and 11.6 to 94.0% for
400 POPA/POPC at $t=24$ h. Under the action of SRPP1, there was no significant difference
401 between the leakages from POPA/POPC and POPG LUV.

402 Both RP proteins interact strongly with negatively charged LUV made of POPA/POPC
403 (1:1) and POPG, as evidenced by the $\sim 70\%$ and $\sim 90\%$ calcein leakage induced by REF1 and
404 SRPP1 for both LUV types, respectively. This suggests that anionic headgroups favor
405 interactions between LUV and RP proteins REF1 and SRPP1. Although both proteins have a
406 net negative charge at pH 7.4 (REF1: -2, SRPP1: -6, [14]), it is interesting to observe that
407 they still interact with negatively charged PL. This phenomenon has also been observed in *T.*
408 *brevicorniculatum*, where several negatively charged SRPP proteins (net charges at pH 7.4
409 are indicated in brackets), *i.e.* Tb-SRPP1 (-9), Tb-SRPP3 (-13), Tb-SRPP4 (-14) and Tb-
410 SRPP5 (-15), have been shown to have a preference for negatively charged PL headgroups
411 [25].

412 We have previously suggested that REF1 and SRPP1 may behave similarly to surfactin
413 [18], a negatively charged antimicrobial peptide (7 amino acids, net charge: -2) that strongly
414 interacts with negatively charged lipids [37]. Surfactin is able to induce a strong
415 destabilization of negatively charged micrometer-scale liposomes, leading to the formation of
416 stable small unilamellar vesicles of a few tens of nanometers. This occurs in two steps. First,
417 peptide inserts into membrane because of favorable van der Waals forces between the acyl
418 chains of lipids and the hydrophobic part of the peptide. Second, electrostatic repulsion
419 occurs between negative charges of lipid headgroups and peptides. This results in severe
420 changes in membrane curvature, leading to the formation of smaller and stable vesicles. This

421 mechanism is known as the ‘electrostatic wedge’ model [37, 38]. The massive disruption of
 422 negatively charged POPG and POPA/POPC LUV by the highly hydrophobic and negatively
 423 charged REF1 and SRPP1 proteins (Figure 2) supports the possibility that these RP proteins
 424 behave in a ‘surfactin-like’ manner, forming both hydrophobic contacts with lipid acyl chains
 425 and electrostatic repulsions with anionic headgroups. These results are consistent with the
 426 literature, which has shown that SRPP can affect the size and stability of RP. For instance,
 427 Hillebrand *et al.* showed that SRPP proteins are essential for maintaining the integrity of RP
 428 in *T. brevicorniculatum* [39]. Indeed, the RP of transgenic plants with strongly reduced
 429 TbSRPP protein level displayed significantly higher diameter as compared to wild-type
 430 plants. This indicates that RP in transgenic plants are less stable, with a heterogeneity in size
 431 that suggests RP fusion. Another study showed that the addition of TbSRPPs to artificial
 432 poly(*cis*-1,4-isoprene) bodies narrowed their size distribution [25]. In *H. brasiliensis*,
 433 Yamashita *et al.* highlighted the role of REF1 in modulating the diameters of washed RP,
 434 providing the first direct evidence that REF1 is an important protein for RP stability [40].

435

436 3. REF1 displays higher affinity than SRPP1 for monolayer of anionic PL

437 The interactions of RP proteins REF1 and SRPP1 were studied with monolayer of PL
 438 formed at the air/buffer interface. The films were characterized by surface pressure,
 439 ellipsometry, BAM and PM-IRRAS spectroscopy. Before investigating these interactions,
 440 isotherms of synthetic PL were recorded while BAM images were regularly captured during
 441 compression (data not shown). All PL isotherms showed a regular increase in surface
 442 pressure without a shoulder until collapse. BAM images showed that the PL films were
 443 homogeneous, without aggregation or segregation. These results indicate the presence of a
 444 single, homogeneous liquid-expanded phase, in agreement with the presence of one
 445 unsaturation in the lipid acyl chains of the studied PL. The minimal mean molecular area of
 446 POPA (50 Å²/molecule), POPC (55 Å²/molecule) and POPG (57 Å²/molecule) were found to
 447 be in agreement with the values reported by Liu *et al.* [35], Smaby and Brockman [41] and
 448 Kwon *et al.* [42], respectively. Due to the smaller size of its headgroup as compared to POPC
 449 and POPG [27], POPA can be compressed to a lower minimal mean molecular area.

450 To prepare PL monolayers for further experiments with proteins, they were compressed to
 451 a surface pressure of 28 mN.m⁻¹ before injecting the protein into the subphase (2 μM). At this
 452 surface pressure, POPA, POPC and POPG have a mean molecular area of 52, 60 and 64
 453 Å²/molecule, respectively. The thicknesses of the PL films compressed at 28 mN.m⁻¹ were
 454 measured by ellipsometry (Table 3, left part) and agree with the values reported in the
 455 literature [30, 43].

456

Synthetic PL	Synthetic PL without protein at $\Pi = 28 \text{ mN.m}^{-1}$		Synthetic PL ($\Pi_i = 28 \text{ mN.m}^{-1}$) with 2 μM proteins at Π_p (plateau)			
			REF1		SRPP1	
	Mean molecular area (Å ² /molecule)	Thickness (Å)	$\Delta\Pi$ (mN/m)	Thickness (Å)	$\Delta\Pi$ (mN/m)	Thickness (Å)
POPC	60	14.3 ± 1.4	6.3 ± 0.9	16.7 ± 1.2	5.4 ± 0.6	16.5 ± 0.2
POPA	52	14.4 ± 0.8	4.2 ± 0.2	77.2 ± 0.8	5.4 ± 0.5	55.7 ± 2.7

POPG	64	15.8 ± 1.6	4.9 ± 0.7	62.2 ± 1.0	6.2 ± 0.7	28.1 ± 0.7
-------------	----	----------------	---------------	----------------	---------------	----------------

457 **Table 3.** Layer thickness at 28 mN.m^{-1} of synthetic PL monolayers made of POPC, POPA and POPG.
 458 Film thickness and increase in surface pressure ($\Delta\Pi$) are also reported when synthetic PL interact with
 459 REF1 and SRPP1 proteins injected at $2 \mu\text{M}$ in TBS 1X buffer pH 7.4.

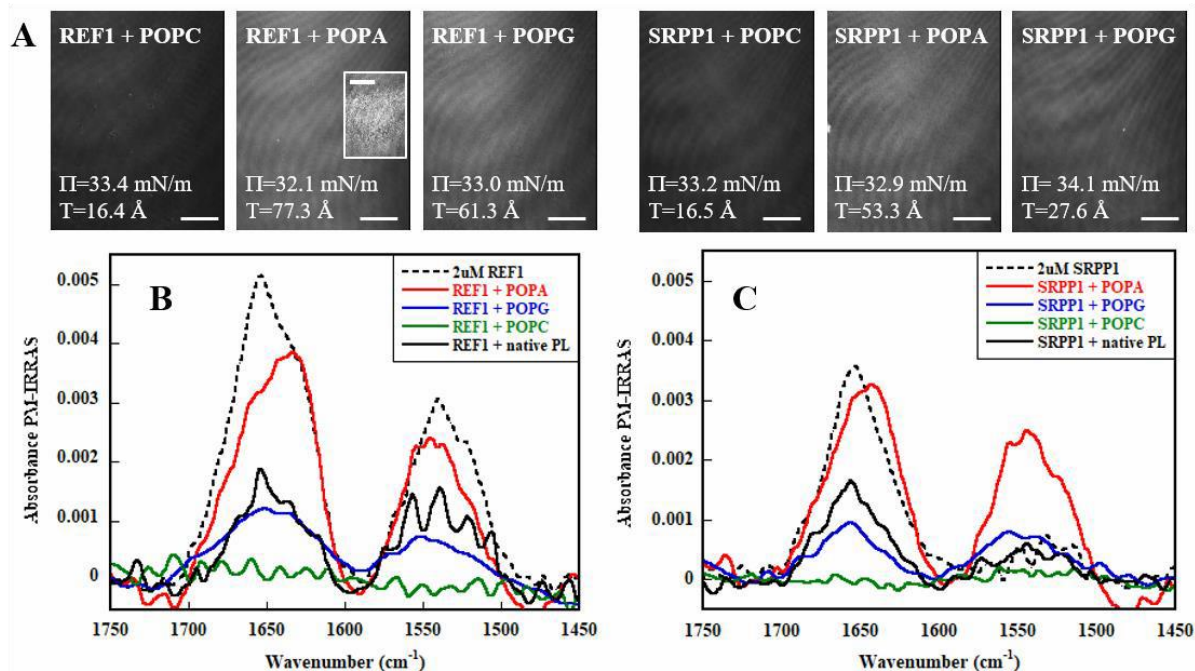
460

461 After protein injection, the surface pressure increased regularly due to the adsorption of
 462 proteins in the synthetic PL monolayers, until it reached a plateau within 10 minutes to 1
 463 hour. The difference between the initial surface pressure of the lipid (Π_i) and the surface
 464 pressure reached at the plateau (Π_p) gives the surface pressure increase ($\Delta\Pi = \Pi_p - \Pi_i$). $\Delta\Pi$
 465 values and thicknesses of lipid/protein films measured at the maximal surface pressure of the
 466 kinetic (plateau) are reported in Table 3 (right part).

467 The surface pressure increase due to REF1 adsorption into PL monolayers was
 468 significantly higher for POPC ($+ 6.3 \text{ mN.m}^{-1}$) than for POPA ($+ 4.2 \text{ mN.m}^{-1}$), while the one
 469 measured for POPG was intermediate ($+ 4.9 \text{ mN.m}^{-1}$) (not significantly different from POPC
 470 or POPG). Surprisingly, the thickness of the REF1/POPC film (16.7 \AA) was almost the same
 471 as that of the pure POPC film (14.3 \AA), resulting in a very small thickness increase ($+ 2.4 \text{ \AA}$).
 472 In contrast, as compared to pure PL films, the thicknesses of the REF1/POPG (62.2 \AA , $+ 46.4$
 473 \AA) and REF1/POPA (77.2 \AA , $+ 62.8 \text{ \AA}$) films were much higher than those of the pure PL
 474 films. For POPC, although the surface pressure increased significantly when REF1 was
 475 injected, the film thickness remained almost unchanged, suggesting that REF1 does not
 476 penetrate into the POPC monolayer. In contrast, the measured thickness increases for POPA
 477 and POPG indicate that REF1 penetrates deeply into POPA and POPG monolayers. BAM
 478 images and PM-IRRAS spectra were recorded at the plateau of the adsorption kinetic of
 479 proteins into PL films (Figure 3). BAM images (Figures 3A) of both REF1/POPG and
 480 REF1/POPC films are homogeneous showing the absence of aggregation. REF1/POPA film
 481 was most of the time homogeneous but white objects were sometimes noticed (insert on
 482 REF1/POPA BAM image in Figure 3A) indicating that aggregation may occur.

483 The PM-IRRAS spectra of films of REF1, REF1/synthetic PL and REF1/native PL (from
 484 [19]) are shown in Figures 3B. The amide II band of REF1 was centered at 1540 cm^{-1} , while
 485 the amide I was intense and centered at 1653 cm^{-1} , with a strong shoulder at 1630 cm^{-1} and
 486 two slight ones at 1670 cm^{-1} and 1690 cm^{-1} . This indicates that several secondary structures
 487 coexist in REF1 when the protein forms a film at the air/buffer interface, *i.e.* mainly α -helices
 488 (1653 cm^{-1}), as well as β -sheets ($1630, 1690 \text{ cm}^{-1}$) and turns (1670 cm^{-1}) [17]. The PM-
 489 IRRAS spectra of REF1 interacting with PL are different from the spectrum of the protein.
 490 They are also dramatically different depending on the lipid type (Figure 3B). No signal was
 491 detected when REF1 interacts with POPC, resulting in a flat spectrum. This result is
 492 consistent with ellipsometry (no thickness increase) and BAM (low level of grey) data. In
 493 contrast to POPC, the PM-IRRAS spectra of REF1/POPG and REF1/POPA films show the
 494 presence of two amide bands. The spectrum of POPG/REF1 was slightly less intense than the
 495 one of REF1 interacting with native PL of *Hevea* latex, but the position of amide bands were
 496 similar for both spectra. The secondary structure of REF1 is unchanged (as compared to pure
 497 REF1 film) when it interacts with POPG, as we previously observed for native PL [19]. The
 498 protein mainly contains α -helices, and the ratios between the intensities of the amide I and
 499 amide II bands are similar for pure REF1 and REF1/POPG. This suggests that the α -helices

500 of REF1 keep the same orientation in the POPG monolayer as they do when the protein is
 501 alone at the interface. Interestingly, the spectrum of REF1/POPA is drastically different from
 502 the one of REF1. The amide I band is shifted 20 cm^{-1} to lower wavenumber (1633 cm^{-1}),
 503 which indicates a high proportion of β -sheets. This means that the secondary structure of
 504 REF1 switches from mainly α -helices to mainly β -sheets when it interacts with POPA lipid.
 505 This observation is consistent with the aggregation observed by BAM (insert in Figure 3A)
 506 and the strong thickness increase (compared to pure lipid film) measured when REF1
 507 accumulates into POPA (Table 3).
 508



509
 510 **Figure 3.** A) BAM images ($450 \times 600 \mu\text{m}^2$) of protein/lipid films captured on the plateau. Surface
 511 pressure (Π) and thickness (T) of the films at the capture are indicated for each image. White bars are
 512 $100 \mu\text{m}$. B) PM-IRRAS spectra in the $1750\text{-}1450 \text{ cm}^{-1}$ spectral range of REF1 and REF1/PL films
 513 recorded at the plateau. C) PM-IRRAS spectra in the $1750\text{-}1450 \text{ cm}^{-1}$ spectral range of SRPP1 and
 514 SRPP1/PL films recorded at the plateau. The spectra recorded for REF1 and SRPP1 interacting with
 515 native PL (from [19]) were reminded on B and C, respectively.
 516

517 The insertion of SRPP1 protein below PL monolayers resulted in surface pressure
 518 increases that were not significantly different between the lipids: $+6.2 \text{ mN}\cdot\text{m}^{-1}$ for POPG and
 519 $+5.4 \text{ mN}\cdot\text{m}^{-1}$ for both POPC and POPA. As observed for REF1, the interaction of SRPP1
 520 with POPC resulted in an almost unchanged thickness of $+2.2 \text{ \AA}$. A strong thickness increase
 521 (as compared to pure PL films) was measured for SRPP1/POPA film ($+41.3 \text{ \AA}$) while the
 522 one of SRPP1/POPG film was intermediate, at $+12.3 \text{ \AA}$. All BAM images (Figure 3A)
 523 indicate that no aggregation was observed when SRPP1 interacts with PL. SRPP1 proteins
 524 adsorb homogeneously in synthetic PL monolayers as observed with native PL of *Hevea*
 525 latex [19].

526 As shown in Figure 3C, PM-IRRAS spectrum of pure SRPP1 displays a sharp and intense
 527 amide I band centered at 1653 cm^{-1} and a weak amide II band at 1530 cm^{-1} corresponding to a
 528 strong structuration of SRPP1 in α -helices lying flat on the interface [17]. Moreover, slight

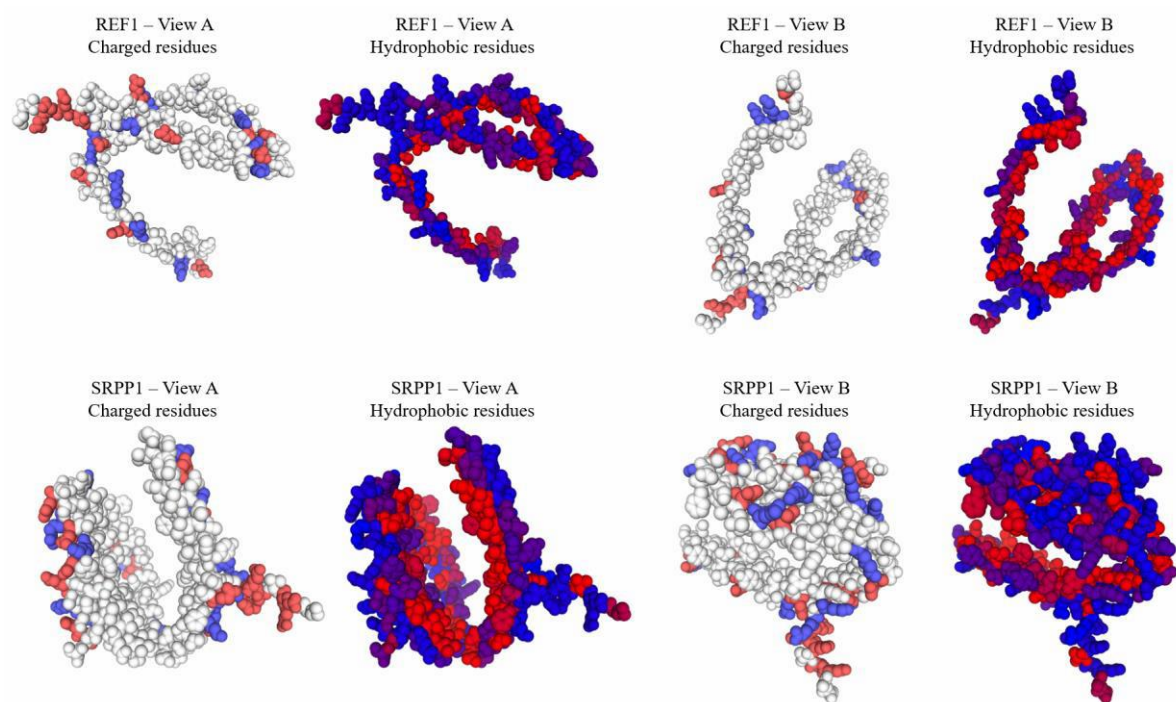
529 shoulders detected at 1630 and 1690 cm^{-1} are the signature of β -sheets. As for REF1/POPC
530 film, a flat PM-IRRAS spectrum was recorded for SRPP1/POPC film. This suggests that
531 SRPP1 does not adsorb at the interface into POPC monolayer, in agreement with the very
532 small thickness increase measured by ellipsometry and the low level of grey of BAM image
533 (Figure 3A). The PM-IRRAS spectrum of SRPP1/POPG showed two amide bands having the
534 same wavenumber as the bands of pure SRPP1 indicating that protein keeps its secondary
535 structure in α -helices when interacting with POPG. However, as compared to the protein
536 alone, the intensities of amide bands of SRPP1 were affected in the presence of POPG. With
537 POPG, the amide II band was almost as intense as the amide I band, indicating that a drastic
538 change of orientation of the α -helices occurred. The α -helices, which adopt a flat orientation
539 with respect to the interface when the protein is alone, reorient themselves more
540 perpendicularly to the interface with POPG lipid. With POPA lipid, a particular behavior was
541 highlighted. The amide I band shifted slightly to lower wavenumber with a moderate shift of
542 amide I toward lower wavenumber (1643 cm^{-1}) and the intensity of the amide II band
543 increased significantly. These observations are the signature of random domains indicating a
544 lower structuration of SRPP1 when interacting with POPA, as compared to pure protein.

545 When both REF1 and SRPP1 were injected below flat monolayers of neutral POPC,
546 despite significant protein-induced increases in surface pressure (Table 3), no amide I or
547 amide II bands could be detected in mixed lipid/protein films (Figures 3B and 3C). This
548 phenomenon (*i.e.* a surface pressure increase associated to a flat PM-IRRAS spectrum) has
549 been previously observed for a tryptophan-rich peptide interacting with DPPC (1,2-
550 dipalmitoyl-sn-glycero-3-phosphocholine) monolayers and authors explained that this
551 behavior could be linked to aromatic tryptophan residues which prefer the water/membrane
552 interface [44]. Similarly, other authors have shown that a penetrating peptide induced a low
553 chain disorder in DPPC monolayer and strongly perturbed the whole lipid structure when
554 10% of anionic DPPS (1,2-dipalmitoyl-sn-glycero-3-phospho-L-serine) was added to DPPC
555 monolayer [45]. In this work, we observed that the grey level of POPC/RP proteins BAM
556 images (Figure 3A) remained low throughout the kinetic while very slight thickness increases
557 were measured (Table 3). These results suggest that both REF1 and SRPP1 do not penetrate
558 in POPC monolayers but instead accumulate below lipid headgroups without interacting with
559 lipid acyl chains. The proximity of proteins to the lipid headgroups might disturb both the
560 lipid headgroup and protein hydration layers, *i.e.*, the regions of structured water molecules
561 that form hydrogen bonds with lipid headgroups and proteins. The surface pressure increase
562 might be a consequence of the strong perturbation of the hydration layer of POPC
563 headgroups. Moreover, the fact that neither REF1 nor SRPP1 interact with POPC tails could
564 also suggest that the hydration of proteins is increased leading to specific structuration which
565 prevents them from adsorbing to the air interface. It was previously observed that an alkaline
566 phosphatase strongly inserts into DPPS (negatively charged) monolayers, while it only
567 interacts with the headgroups of DPPC [46]. Different protein hydration layers between the
568 DPPC and DPPS monolayers have been suggested to explain these results. These authors
569 later showed that an increase in the hydration of this protein results in a lower PM-IRRAS
570 signal [47]. In this work, the perturbation of lipid headgroup and protein hydration layers
571 could respectively explain the increase in surface pressure and the lack of amide bands on

572 PM-IRRAS spectra. In a previous study with DMPC (1,2-dimyristoyl-sn-glycero-3-
573 phosphocholine) monolayer at 28 mN.m^{-1} , no PM-IRRAS signal and no surface pressure
574 increase were noticed for SRPP1. In contrast, amide bands were detected for REF1 as well as
575 important surface pressure and thickness increases ($+9.8 \text{ mN.m}^{-1}$ and $+47 \text{ \AA}$, respectively)
576 [14]. These differences are not fully understood, but could arise from different lipid species
577 (POPC (16:0-18:1 PC) vs DMPC (14:0-14:0 PC)) and/or varying experimental conditions
578 (temperature, humidity).

579 In contrast to neutral POPC, RP proteins REF1 and SRPP1 developed strong interactions
580 with negatively charged PL monolayers, as indicated by surface pressure, ellipsometry, BAM
581 and PM-IRRAS data. Thus, as observed for curved PL membrane (LUV), anionic PL seem to
582 promote interactions with RP proteins. This might seem counterintuitive as both REF1 and
583 SRPP1 proteins are negatively charged at physiological pH. However, this phenomenon is
584 commonly observed for antimicrobial peptides which have the ability to adopt a shape in
585 which clusters of hydrophobic and cationic amino acids are spatially organized in discrete
586 sectors of the molecule [48]. REF1 and SRPP1 proteins contain 8.7% and 9.3% of positively
587 charged amino acids, respectively; as well as 10.0% and 12.2% of negatively charged amino
588 acids, respectively. The structures of REF1 (GenBank accession no. P15252) and SRPP1
589 (GenBank accession no. O82803) predicted by DeepMind's AlphaFold [49, 50] are shown in
590 Figure 4. Although these views are predictions and do not necessarily represent possible
591 protein folding when they interact with other molecules, they highlight clustering of
592 hydrophobic residues in specific regions of both proteins. Regarding charged amino acids,
593 there is no clear clustering of positive and negative residues in REF1 and SRPP1 structures
594 but some protein folding might occur in the presence of anionic PL monolayers to create
595 pockets or surfaces of positively charged residues which might promote contacts with anionic
596 lipids, as described for various proteins [51]. In this work, while protein adsorption might be
597 first enhanced by electrostatic interactions between positive pockets of protein residues and
598 lipid headgroups, hydrophobic contacts might then dominate between hydrophobic surfaces
599 of proteins and acyl chains of lipids.

600



601
 602 **Figure 4.** Structures of proteins REF1 (GenBank accession no. P15252) and SRPP1 (GenBank
 603 accession no. O82803) predicted by DeepMind's AlphaFold (average model confidence: 72.43 and
 604 69.83 for REF1 and SRPP1, respectively). Two different views (A and B) are shown for each protein,
 605 as well as two different representations for each view where charged residues (color code: blue =
 606 positive residues Arginine + Lysine, red = negative residues Asparagine + Glutamate) and
 607 hydrophobic residues (color code: blue = least hydrophobic, red = most hydrophobic) are highlighted.

608
 609 When comparing the behavior of REF1 and SRPP1 with anionic PL, the surface pressure
 610 increases were not significantly different while thickness increases were much higher for
 611 REF1 than SRPP1 with both POPA and POPG. This indicates a stronger affinity of REF1
 612 than SRPP1 for flat negatively charged PL membranes. They also agree with previous works
 613 where SRPP1 was shown to interact preferentially with headgroups of native and synthetic
 614 PL with no deep insertion of the protein into the monolayer [18, 19]. Interestingly, as
 615 compared to POPG, both RP proteins interact more strongly with POPA. The smaller
 616 phosphate headgroup of POPA may facilitate hydrophobic interactions between the
 617 hydrophobic domains of the proteins and the lipid acyl chains. For both proteins, the surface
 618 pressure increases with POPA were not significantly different from POPG. While both
 619 proteins keep their structures (α -helices) with POPG, they accumulate much more into POPA
 620 where they also underwent changes in their secondary structure: a destructure for SRPP1
 621 and a variation from α -helices to β -sheets for REF1. Some aggregation was noticed when
 622 REF1 interacts with POPA. This behavior (*i.e.* shift from α -helices to β -sheets + aggregation)
 623 was already observed when REF1 interacts with native neutral lipids from *Hevea* latex and
 624 we proposed that the strong aggregation of REF1 with neutral lipids might have a significant
 625 impact on the irreversibility of coagulation of rubber particles [19]. Dupont *et al.* studied the
 626 PL composition of the membrane of lutoids from *Hevea* and reported a high content of
 627 phosphatidic acid (> 80% of total lutoid PL), which makes lutoids highly electronegatively
 628 charged particles [26]. The authors suggested that small, localized drops in the

629 electronegative charge of the lutoids, by combination with cations or by other mechanisms,
630 could facilitate the aggregation of rubber particles onto the lutoid surface. These biochemical
631 mechanisms may be enhanced by physical mechanisms related to the behavior of REF1 with
632 POPA described in this work, *i.e.* switch of REF1 structure from α -helices to β -sheets and
633 protein aggregation. The increase in β -sheets was shown to be associated to the amyloid form
634 of REF1 [17], while negatively charged lipids were reported to favor interactions and
635 aggregation of amyloid proteins [52]. From this study, we propose that the interactions of
636 REF1 with phosphatidic acid-enriched lutoid membranes might result in a switch of REF1
637 structure to its amyloid aggregated form that could be involved, in synergy with biochemical
638 mechanisms, in the irreversible coagulation mechanism of *Hevea* RP.

639

640

CONCLUSION

641 REF1 and SRPP1, two major proteins from *Hevea* latex localized at the surface of rubber
642 particles, were studied for their interactions with three synthetic PL in the form of vesicles
643 and monolayers. According to the acyl chain and headgroup compositions of native PL from
644 *Hevea* latex, three synthetic PL were selected, *i.e.* POPA, POPC and POPG.

645 For both proteins, lower calcein leakages were measured from zwitterionic LUV (POPC)
646 than from anionic LUV (POPA/POPC and POPG). This suggests that LUV/protein
647 interactions might be initiated by electrostatic interactions between positive pockets of
648 protein residues and negatively charged lipid headgroups. The disruption of both zwitterionic
649 and anionic LUV (120 nm) was faster and stronger for SRPP1 than REF1. This might reflect
650 the preference of SRPP1 for binding to smaller RP and could explain why SRPP1 and REF1
651 mostly bind to SRP ($< 0.2 \mu\text{m}$) and LRP ($> 0.3 \mu\text{m}$), respectively [53].

652 Protein/lipid interactions were studied at the air/liquid interface by forming PL monolayers
653 at the interface. As observed in LUV systems, both proteins interacted much weakly with
654 POPC as compared to anionic PL monolayers. We suggested that RP protein do not penetrate
655 in POPC monolayers but instead accumulate below lipid headgroups, supposedly due to the
656 perturbation of the lipid headgroup and protein hydration layers [44-47]. In LUV systems, the
657 interactions of REF1 with POPC was almost absent while they were moderate for SRPP1.
658 The different behavior of SRPP1 protein when it interacts with a planar lipid monolayer or a
659 curved LUV reveals the impact of the membrane curvature.

660 As compared to zwitterionic POPC, both proteins interacted more strongly with anionic
661 monolayers made of POPA and POPG, with stronger interactions for REF1 than SRPP1. It is
662 believed that pockets or surfaces of positively charged residues in the protein sequences
663 might promote contacts with anionic lipids [51]. As compared to POPG, POPA induced a
664 stronger accumulation of proteins. POPA also induced a destructure of the SRPP1
665 structure and a specific behavior of REF1 with some aggregation and a switch of its structure
666 from α -helices to β -sheets. This behavior was already observed when REF1 interacts with
667 native neutral lipids from *Hevea* latex and we suggested that the strong aggregation of REF1
668 with neutral lipids might have a significant impact on the irreversibility of coagulation of
669 rubber particles [19].

670 This work reinforces the proposed physical role of REF1 (*i.e.* switch of structure) in the
671 irreversible coagulation of latex. Indeed, the interactions of REF1 with phosphatidic acid-

672 enriched luteoid membranes [26], could also result in a switch of REF1 structure to its amyloid
 673 aggregated form that would be involved, in synergy with biochemical mechanisms, in the
 674 irreversible coagulation mechanism of *Hevea* RP. Moreover, this study highlights the
 675 important role of lipid nature in modulating the behavior and structuration of both REF1 and
 676 SRPP1 proteins which probably indirectly affects their function in rubber tree [14].

677 678 **ACKNOWLEDGMENTS**

679 The authors thank ANR (Agence Nationale de la Recherche, RUBBEx project N°14-CE07-
 680 0026-02), KURDI, (Kasetsart University, project N°120.58), Campus France (Ministères des
 681 Affaires Etrangères et de l'Enseignement Supérieur et de la Recherche) and OHEC (Office of
 682 the Higher Education Commission, Thailand) (PHC SIAM 2014: project N°31786VJ) for
 683 funding this research. Agropolis Fondation is also thanked for the support to the creation of
 684 LipPolGreen-Asia platform in Kasetsart Agricultural and Agro-Industrial Product
 685 Improvement Institute, Bangkok. The authors are thankful to Dr. Berthelot for protein
 686 production and to Visahakit Thai Rubber Co. Ltd. for providing latex in their plantation. This
 687 work was undertaken as part of the Hevea Research Platform in Partnership (HRPP).

688 689 **ABBREVIATIONS**

690 BAM, Brewster angle microscopy; CCD, charge-coupled device; DMPC, 1,2-dimyristoyl-sn-
 691 glycerol-3-phosphocholine; DPPC, 1,2-dipalmitoyl-sn-glycerol-3-phosphocholine; DPPS, 1,2-
 692 dipalmitoyl-sn-glycerol-3-phospho-L-serine; FA, Fatty acid; FAME, fatty acid methyl ester;
 693 GL, glycolipid; LRP, large rubber particle; LUV: large unilamellar vesicle, Nd:YAG,
 694 neodymium-doped yttrium aluminium garnet; NL, neutral lipid; NR, natural rubber; PA,
 695 phosphate; PC, phosphocholine; PE, phosphoethanolamine; PG, phosphoglycerol; PL,
 696 phospholipid; POPA, 1-palmitoyl-2-oleoyl-sn-glycerol-3-phosphate; POPC, 1-palmitoyl-2-
 697 oleoyl-sn-glycerol-3-phosphocholine; POPG, 1-palmitoyl-2-oleoyl-sn-glycerol-3-
 698 phosphoglycerol; PM-IRRAS, polarization modulated-infrared reflection adsorption
 699 spectroscopy; REF, rubber elongation factor; SPE, Solid Phase Extraction; SRP, small rubber
 700 particle; SRPP, small rubber particle protein; TBS, tris-buffered saline.

701 702 **REFERENCES**

- 703 [1] K. Cornish, *et al.*, Rubber particles from four different species, examined by transmission
 704 electron microscopy and electron-paramagnetic-resonance spin labeling , are found to consist
 705 of a homogeneous rubber core enclosed by a contiguous, monolayer biomembrane, *Planta*
 706 210 (1999) 85-96.
 707 [2] D.J. Siler, *et al.*, Composition of rubber particles of *Hevea brasiliensis*, *Parthenium*
 708 *argentatum*, *Ficus elastica*, and *Euphorbia lactiflua* indicates unconventional surface
 709 structure, *Plant Physiol. Biochem.* 35 (1997) 881-889.
 710 [3] K. Nawamawat, *et al.*, Surface nanostructure of *Hevea brasiliensis* natural rubber latex
 711 particles, *Colloids and Surfaces A: Physicochemical and Engineering Aspects* 390 (2011)
 712 157-166.
 713 [4] S. Kumarn, *et al.*, Investigating the mechanistic and structural role of lipid hydrolysis in
 714 the stabilization of ammonia-preserved *Hevea* rubber latex, *Langmuir* 34 (2018) 12730-
 715 12738.

- 716 [5] C. Bottier, Biochemical composition of *Hevea brasiliensis* latex: A focus on the protein,
717 lipid, carbohydrate and mineral contents, in: R. Nawrot (Ed.), Advances in Botanical
718 Research. Latex, Laticifers and Their Molecular Components - From Functions to Possible
719 Applications, Elsevier Ltd 2020, pp. 201-237.
- 720 [6] A.P. Singh, *et al.*, The micromorphology and protein characterization of rubber particles
721 in *Ficus carica*, *Ficus benghalensis* and *Hevea brasiliensis*, Journal of Experimental Botany
722 54 (2003) 985-992.
- 723 [7] D.F. Wood, K. Cornish, Microstructure of purified rubber particles, International Journal
724 of Plant Sciences 161 (2000) 435-445.
- 725 [8] J. Wu, *et al.*, Super-Resolution Fluorescence Imaging of Spatial Organization of Proteins
726 and Lipids in Natural Rubber, Biomacromolecules 18 (2017) 1705-1712.
- 727 [9] L. Dai, *et al.*, In-depth proteome analysis of the rubber particle of *Hevea brasiliensis* (para
728 rubber tree), Plant molecular biology 82 (2013) 155-168.
- 729 [10] M.S. Dennis, D.R. Light, Rubber elongation factor from *H. brasiliensis*, The Journal of
730 Biological Chemistry 264 (1989) 18608-18617.
- 731 [11] S.K. Oh, *et al.*, Isolation, characterization, and functional analysis of a novel cDNA
732 clone encoding a small rubber particle protein from *Hevea brasiliensis*, Journal of Biological
733 Chemistry 274 (1999) 17132-17138.
- 734 [12] H.Y. Yeang, *et al.*, The 14.6 kd rubber elongation factor (Hev b 1) and 24 kd (Hev b 3)
735 rubber particle proteins are recognized by IgE from patients with spina bifida and latex
736 allergy, Journal of Allergy and Clinical Immunology 98 (1996) 628-639.
- 737 [13] F. Kuroiwa, *et al.*, Reconstitution of prenyltransferase activity on nanodiscs by
738 components of the rubber synthesis machinery of the *Para* rubber tree and guayule, Scientific
739 Reports 12 (2022) 3734.
- 740 [14] K. Berthelot, *et al.*, *Hevea brasiliensis* REF (Hevb1) and SRPP (Hevb3): an overview of
741 possible functions of rubber particle proteins, Biochimie 106 (2014) 1-9.
- 742 [15] C. Tang, *et al.*, The rubber tree genome reveals new insights into rubber production and
743 species adaptation, Nature Plants 2 (2016) 16073.
- 744 [16] J. Sarkis, V. Vié, Biomimetic models to investigate membrane biophysics affecting lipid
745 – protein interaction, Frontiers in Bioengineering and Biotechnology 8 (2020) 270.
- 746 [17] K. Berthelot, *et al.*, Rubber elongation factor (REF), a major allergen component in
747 *Hevea brasiliensis* latex has amyloid properties, PloS One, 2012, p. e48065.
- 748 [18] K. Berthelot, *et al.*, Rubber particle proteins, HbREF and HbSRPP, show different
749 interactions with model membranes, BBA - Biomembranes, 2014, pp. 287-299.
- 750 [19] K. Wadeesirisak, *et al.*, Rubber particle proteins REF1 and SRPP1 interact differently
751 with native lipids extracted from *Hevea brasiliensis* latex, BBA Biomembranes 1859 (2017)
752 201-210.
- 753 [20] E. Reszczyńska, A. Hanaka, Lipids composition in plant membranes, Cell Biochemistry
754 and Biophysics 78 (2020) 401-414.
- 755 [21] H. Hasma, A. Subramaniam, Composition of lipids in latex of *Hevea brasiliensis* clone
756 RRIM 501, Journal of Natural Rubber Research 1 (1986) 30-40.
- 757 [22] S. Liengprayoon, *et al.*, Lipid compositions of latex and sheet rubber from *Hevea*
758 *brasiliensis* depend on clonal origin, Europ. J. Lipid Sci. Tech. 115 (2013) 1021-1031.
- 759 [23] S. Liengprayoon, *et al.*, Distribution of the non-isoprene components in the four *Hevea*
760 *brasiliensis* latex centrifugation fractions, Journal of Rubber Research 24 (2021) 759-769.
- 761 [24] H. Hasma, Lipids associated with rubber particles and their possible role in mechanical
762 stability of latex concentrates, Journal of Natural Rubber Research 6 (1991) 105-114.
- 763 [25] N. Laibach, *et al.*, Small rubber particle proteins from *Taraxacum brevicorniculatum*
764 promote stress tolerance and influence the size and distribution of lipid droplets and artificial
765 poly(*cis*-1,4-isoprene) bodies, The Plant Journal 93 (2018) 1045-1061.

- 766 [26] J. Dupont, *et al.*, Phospholipid composition of the membrane of luteoids from *Hevea*
767 *brasiliensis* latex, *Phytochemistry* 15 (1976) 1215-1217.
- 768 [27] A. Dickey, R. Faller, Examining the contributions of lipid shape and headgroup charge
769 on bilayer behavior, *Biophysical Journal* 95 (2008) 2636-2646.
- 770 [28] G. Rouser, *et al.*, Two Dimensional thin layer chromatographic separation of polar lipids
771 and determination of phospholipids by phosphorus analysis of spots values obtained in
772 quadruplicate determinations of different amounts of phosphorus, *Lipids* 5 (1970) 494-496.
- 773 [29] R.M.A. Azzam, N.M. Bashara, Ellipsometry and Polarized Light, in: E.S. Ltd (Ed.)
774 North- Holland Physica Publishing, New York, 1987.
- 775 [30] H.P. Ta, *et al.*, Comparative studies of nontoxic and toxic amyloids interacting with
776 membrane models at the air-water interface, *Langmuir* 27 (2011) 4797-4807.
- 777 [31] D. Blaudez, *et al.*, Investigations at the air/water interface using polarization modulation
778 IR spectroscopy, *Journal of the Chemical Society, Faraday Transactions* 92 (1996) 525-530.
- 779 [32] R.M.B. Moreno, *et al.*, Technological properties of latex and natural rubber of *Hevea*
780 *brasiliensis* clones, *Scientia Agricola* 62 (2005) 122-126.
- 781 [33] X. Cong, *et al.*, Allosteric modulation of protein-protein interactions by individual lipid
782 binding events, *Nature Communications* 8 (2017) 2203.
- 783 [34] K. Mladenova, *et al.*, Interaction of Bestrophin-1 with 1-palmitoyl-2-oleoyl-sn-glycero-
784 3-phosphocholine (POPC) in surface films, *Colloids and Surfaces B: Biointerfaces* 122
785 (2014) 432-438.
- 786 [35] W. Liu, *et al.*, Lipid compositions modulate fluidity and stability of bilayers:
787 Characterization by surface pressure and sum frequency generation spectroscopy, *Langmuir*
788 29 (2013) 15022-15031.
- 789 [36] D. Marsh, *Handbook of Lipid Bilayers* (2nd ed.), CRC Press, Boca Raton, 2013.
- 790 [37] S. Buchoux, *et al.*, Surfactin-triggered small vesicle formation of negatively charged
791 membranes: A novel membrane-lysis mechanism, *Biophysical Journal* 95 (2008) 3840-3849.
- 792 [38] E.J. Dufourc, *et al.*, Membrane interacting peptides: from killers to helpers, *Current*
793 *Protein & Peptide Science* 13 (2012) 620-31.
- 794 [39] A. Hillebrand, *et al.*, Down-regulation of small rubber particle protein expression affects
795 integrity of rubber particles and rubber content in *Taraxacum brevicorniculatum*, *PLoS One*
796 7(7) (2012) e41874.
- 797 [40] S. Yamashita, *et al.*, Identification and reconstitution of the rubber biosynthetic
798 machinery on rubber particles from *Hevea brasiliensis*, *Elife* 5 (2016).
- 799 [41] J.M. Smaby, H.L. Brockman, Miscibility, chain packing, and hydration of 1-palmitoyl-
800 2-oleoyl phosphatidylcholine and other lipids in surface phases, *Biophysical journal* 48
801 (1985) 701-707.
- 802 [42] N.H. Kwon, *et al.*, Lipid-bonded conducting polymer layers for a model biomembrane:
803 Application to superoxide biosensors, *Analytical Chemistry* 78 (2006) 52-60.
- 804 [43] D.E. Elmore, Molecular dynamics simulation of a phosphatidylglycerol membrane,
805 *FEBS Letters* 580 (2006) 144-148.
- 806 [44] G. Matar, F. Besson, Influence of the lipid composition of biomimetic monolayers on the
807 structure and orientation of the gp41 tryptophan-rich peptide from HIV-1, *Biochim Biophys*
808 *Acta* 1808(10) (2011) 2534-43.
- 809 [45] E. Bellet-Amalric, *et al.*, Interaction of the third helix of Antennapedia homeodomain
810 and a phospholipid monolayer, studied by ellipsometry and PM-IRRAS at the air-water
811 interface, *Biochim Biophys Acta* 1467 (2000) 131-143.
- 812 [46] F. Ronzon, *et al.*, Behavior of a GPI-anchored protein in phospholipid monolayers at the
813 air-water interface, *Biochim Biophys Acta* 1560 (2002) 1-13.
- 814 [47] F. Ronzon, *et al.*, Structure and orientation of a glycosylphosphatidyl inositol anchored
815 protein at the air/water interface, *J. Phys. Chem.* 106 (2002) 3307-3315.

- 816 [48] M. Zasloff, Antimicrobial peptides of multicellular organisms, *Nature* 415 (2002) 389-
817 395.
- 818 [49] J. Jumper, *et al.*, Highly accurate protein structure prediction with AlphaFold, *Nature*
819 596(7873) (2021) 583-589.
- 820 [50] M. Varadi, *et al.*, AlphaFold Protein Structure Database: massively expanding the
821 structural coverage of protein-sequence space with high-accuracy models, *Nucleic Acids Res*
822 50 (2022) D439-D444.
- 823 [51] L. Li, *et al.*, Ionic protein-lipid interaction at the plasma membrane: what can the charge
824 do?, *Trends Biochem Sci* 39 (2014) 130-40.
- 825 [52] A. Relini, *et al.*, Probing the interplay between amyloidogenic proteins and membranes
826 using lipid monolayers and bilayers, *Adv Colloid Interface Sci* 207 (2014) 81-92.
- 827 [53] A.R.S. Bahri, S. Hamzah, Immunocytochemical localisation of rubber membrane protein
828 in *Hevea* latex, *Journal of Natural Rubber Research* 11 (1996) 88-95

829

